ELSEVIER

Journal of Structural Geology 28 (2006) 444–455

JOURNAL OF STRUCTURAL GEOLOGY

www.elsevier.com/locate/jsg

Serial parallel folding with friction: a primitive model using cubic B-splines

G.W. Hunt [a,*], R. Edmunds [a], C.J. Budd [a], J.W. Cosgrove [b]

[a] *Centre for Nonlinear Mechanics, University of Bath, Bath BA2 7AY, UK*

[b] *Department of Earth Science and Engineering, Royal School of Mines, Imperial College of Science, Technology and Medicine, London SW7 2AZ, UK*

Received 9 July 2004; received in revised form 11 November 2005; accepted 24 November 2005

Available online 24 January 2006

Abstract

An earlier nonlinear model for two-layer parallel folding with bedding plane slip is extended to embrace serial buckling behaviour. Approximating the folds using two cubic B-splines, a quasi-energy formulation admits both synchronous and serial-type buckling under conditions of both controlled load and controlled end-shortening. In the early stages of evolution, non-periodic saddle points, corresponding to localized folds, are found to provide the preferred solution. However, as the end-shortening increases, the saddle points converge with unstable maxima representing synchronous folding, until only periodic solutions exist. This shift from localized to two-hump periodic behaviour is seen as a primitive exposition of the more general theme of serial or sequential fold formation.

Keywords: Layered structures; Localization; Nonlinear response; Buckling; Energy Methods; Instability

1. Introduction

This paper presents a rigorous analysis of serial folding, a process long recognised by geologists as occurring in rocks, but which has not yet been put on a sound mechanical basis. Field observations (Price, 1970, 1975) and analogue experiments (Cobbold, 1975; Blay et al., 1977) have established that serial folding is a common phenomenon in the folding of rocks and it is therefore appropriate to seek a mathematical explanation for this type of behaviour. Fig. 1 shows four stages in an experiment on layers of A4 size paper held together transversely under an applied overburden pressure and compressed in the longitudinal direction by slow application of end displacement to initiate a sequence of parallel folds spreading from the loaded edge. More details can be found in Edmunds et al. (2006). The behaviour shown in Fig. 1 is known variously as sequential amplification (Price and Cosgrove, 1990), serial folding (Blay et al., 1977) or cellular buckling (Hunt et al., 2000). Although the humps form sequentially, it is important to note that the load transfers through the length of the sample without reduction and is not being applied sequentially. The behaviour then differs fundamentally from its spontaneously occurring counterpart (Hunt, 2006), with the resulting wavelengths expected to be different for instance (Budd et al., 2001).

In this paper an analysis is presented for the buckling of a confined multilayer subjected to either a constant external stress or a constant external strain. It complements the work of Biot (1961), Ramberg (1961) and Johnson (1977) in that, unlike these earlier studies, it addresses the problems of the sequential formation of folds rather than spontaneous amplification. Biot (1961) analysed the buckling behaviour of a linear elastic layer set in a viscous matrix. He developed the idea of a dominant wavelength, which amplifies more rapidly than any other, and predicted the formation of a uniform wave-train of sinusoidal buckles. He also studied multilayered elastic models (Biot, 1963, 1964) and reached similar conclusions, namely that a dominant fold wavelength develops and that folding occurs uniformly throughout the model. Ramberg (1961, 1964) analysed the buckling behaviour of both single and multilayered elastic and viscous systems and reached the same conclusions, i.e. that the buckling occurred uniformly throughout the material. These results are in marked contrast to those of the analysis described in this paper, and the buckling behaviour that occurred in the experimental analogue models.

The paper extends a previous study of non-linear folding of a two layer system with bedding plane slip (Budd et al., 2003), and employs the concept of approximating the folding patterns by using cubic B-splines, which allows for two successive humps of different amplitude to be represented and thence can portray primitive forms of both localized and periodic

* Corresponding author.
E-mail address: g.w.hunt@bath.ac.uk (G.W. Hunt).

0191-8141/$ - see front matter © 2005 Elsevier Ltd. All rights reserved.
doi:10.1016/j.jsg.2005.11.006

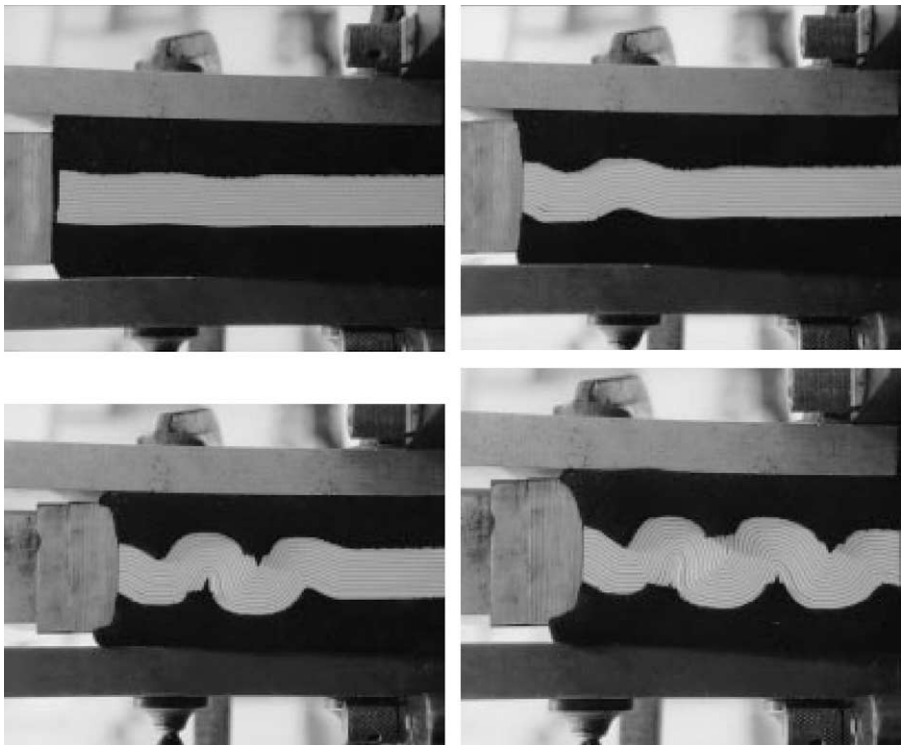

Fig. 1. Parallel folding in layers of paper, showing the serial buckling behaviour.

buckling. We present a rigorous analysis of the process of serial folding in this model, tracking its development and successfully mirroring the sequence seen in Fig. 1, from buckling into a single hump through to the development of the two-hump 'periodic' form as the external loading is changed. Previous work on multilayer buckling by Latham (1985a,b) has confirmed that the localization of folds requires non-linear behaviour, which is built into the model both through the expression for interlayer slip and through a restiffening foundation. The process of bedding plane slip is modelled by allocating frictional properties to the bedding planes owing to the layers being under high overburden pressures (Hobbs et al., 1976). This process is commonly indicated by slickensides, or crystal fibres, on folded bedding planes, and by displaced markers. Remarkably the theory predicts that this slip will occur episodically. Such stick-slip displacement is a process that has been recognized in nature and extensively discussed in the geological literature both with respect to movement along faults and along bedding planes during fold amplification (Hobbs et al., 1976; Price and Cosgrove, 1990). However, this process has not yet been successfully incorporated into any analysis of buckling and we make a systematic derivation in this paper.

Two solutions to the buckling problem are discussed, one relevant to serial folding and the other to spontaneous folding and we show that the type of folding that occurs is controlled by the boundary conditions. Interestingly, the theory confirms that these two folded patterns have different wavelengths.

The problem of the rheology of rocks during folding is also addressed in the paper and the authors agree with previous workers who have argued that elastic buckling solutions are geologically important for predicting fold initiation even when fold amplification is achieved by non-elastic (e.g. viscous or plastic) behaviour. Parallel folds, in particular, are usually found in the upper levels of the Earth's crust, typically in the upper part of an orogenic belt, and this observation supports the use of elasticity theory to study the deformation (de Sitter, 1964).

2. Two layer model

The model is essentially that of two extended elastic beams, held in contact by overburden pressure, but which can slip over each other. If we consider incompressible layers of thickness t, with bending stiffness EI, embedded in a soft foundation of stiffness k per unit length and compressed by a load P (see Fig. 2), and follow classical Euler beam theory, the total

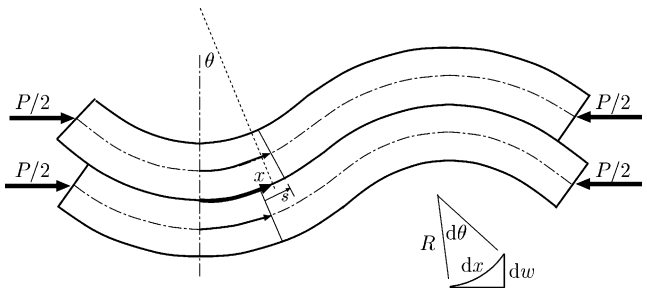

Fig. 2. Slip between incompressible layers constrained to remain in contact.

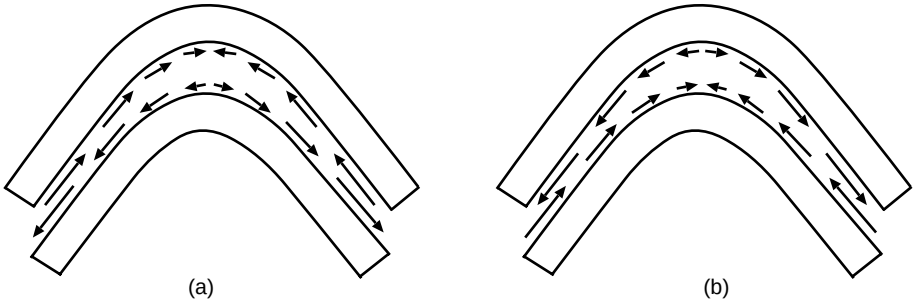

Fig. 3. Slip directions for (a) $\chi=+1$, (b) $\chi=-1$. Note that arrows used to represent frictional forces would be in the reverse directions to those shown.

potential energy, over the half-wavelength L, for small vertical deflections w, can be written as (Budd et al., 2003):

$$V=\int_0^L\left(EI\dot{w}^2-P\frac{\dot{w}^2}{2}+k\frac{w^2}{2}+\chi\mu qt|\dot{w}|\right)\mathrm{d}x \tag{1}$$

where dots denote differentiation with respect to the axial coordinate x. Here the first term is the bending energy in the two layers, the second is the work done by the total load P, the third is the work done in the foundation and the fourth is the work done against friction. The two layers are held together by overburden pressure q, and the coefficient of friction is μ.

The term $\chi=\pm1$ is a *friction indicator*, the purpose of which is to distinguish between the two possibilities of Fig. 3 with the friction acting either to resist growth ($\chi=+1$) or decay ($\chi=-1$) in the amplitude of the buckle. As both situations can appear in the equilibrium paths of the system, the value of χ is adjusted accordingly such that the work done against friction is always positive. The equilibrium solutions of the system on the verge of slipping are then stationary points of the energy functional (1) (for more details see Budd et al. (2003)). Serial buckling arises when an unstable localized response is followed by restabilization and eventual lockup and hence in addition to the terms in Eq. (1) a nonlinearity is included via the extra term:

$$\frac{1}{4}C\int_0^L w^4\mathrm{d}x \tag{2}$$

where C adds a stiffening nonlinear component to the linear foundation stiffness k.

From the experiment in Fig. 1, we see that towards the centre of the multilayer the folds look approximately sinusoidal. Budd et al. (2003) use this as an assumption as to the waveshape and introduce a Rayleigh/Galerkin approximation based on the function

$$w(x)=Q\cos\left(\frac{\pi x}{L}\right)$$

where Q represents the amplitude of the periodic mode-shape. The coefficient of friction μ and the friction indicator χ can then be seen in the role of an imperfection, 'unfolding' the classical bifurcation point, associated with the Euler load, at $Q=0$ and $P=P^C$ (see Fig. 4). At constant load P, points between the curves defined by $\chi=-1$ (or $+1$) are stationary positions where the system is 'trapped' or 'jammed' between the two critical slip conditions, i.e. the friction is holding the layers such that they cannot slip. Points within the jammed region imply that the system is in equilibrium and can be represented by a value of χ somewhere in the range $-1<\chi<1$. Under dead loading (parametric variation in load), falling paths in the upper two quadrants on the edge of the jammed region would be unstable, such that the system would immediately start to deflect from such a point with $|Q|$ increasing (Thompson and Hunt, 1973). The same equilibrium positions are likely to be stable under conditions of rigid loading (parametric variation in end-shortening), however, and would in any case restabilize when the path starts to curve back up as $|Q|$ increases. We note that with a linear foundation ($C=0$) this restabilization never takes place, the paths simply approaching asymptotically a flat (horizontal) path that crosses the P-axis at the critical bifurcation load $P=P^C$ (Budd et al., 2003) and the amplitude grows ad infinitum.

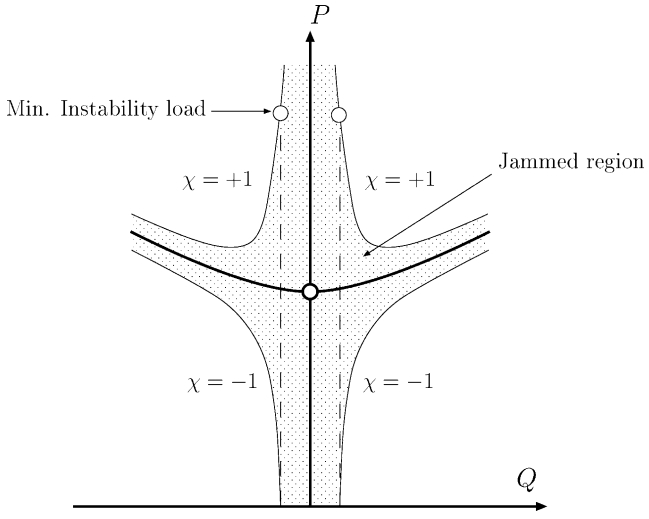

Fig. 4. Bifurcation diagram indicating jammed region for constant μ.

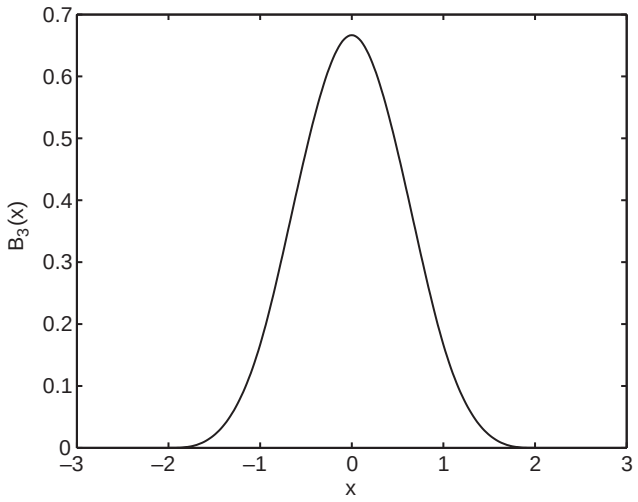

Fig. 5. The cubic B-spline.

3. Modelling waveshapes using cubic B-splines

3.1. The cubic B-spline

To avoid discontinuities in slopes and bending moments, the shape function w should have continuous first and second derivatives. The cubic B-spline, B_3 (see Fig. 5) has this necessary property, but allows discontinuities in the third derivative to give the step changes in shear force seen in Budd et al. (2003). A single cubic spline $B_3(x)$ has the deflected shape

$$B_3(x) = \begin{cases} 0 & x \le -2 \\ \frac{4}{3} + 2x + x^2 + \frac{x^3}{6} & -2 \le x \le -1 \\ \frac{2}{3} - x^2 - \frac{x^3}{2} & -1 \le x \le 0 \\ \frac{2}{3} - x^2 + \frac{x^3}{2} & 0 \le x \le 1 \\ \frac{4}{3} - 2x + x^2 - \frac{x^3}{6} & 1 \le x \le 2 \\ 0 & x \ge 2 \end{cases} \tag{3}$$

Unlike the sinusoidal waveshape approximation, the deflection of the cubic B-spline, together with its first and second derivatives, is zero at both ends. Thus we are able to model a long system that is predominantly unbuckled, but which has a single fold that matches smoothly to the flat (undeflected) state as in a classical homoclinic or localized solution (Champneys et al., 1999).

3.2. Single B-spline formulation

Following the Galerkin approximation of Budd et al. (2003), the deflection, w, can be modelled with a single cubic B-spline. To remain consistent with the earlier work, B_3 is rescaled to the range $0 \le x \le L$, and an amplitude variable, Q, is introduced on the waveshape:

$$w = Q \begin{cases} \frac{4}{3} + \frac{4(2x-L)}{L} + \frac{4(2x-L)^2}{L^2} + \frac{4(2x-L)^3}{3L^3} & 0 \le x \le \frac{L}{4} \\ \frac{2}{3} - \frac{4(2x-L)^2}{L^2} - \frac{4(2x-L)^3}{3L^3} & \frac{L}{4} \le x \le \frac{L}{2} \\ \frac{2}{3} - \frac{4(2x-L)^2}{L^2} + \frac{4(2x-L)^3}{3L^3} & \frac{L}{2} \le x \le \frac{3L}{4} \\ \frac{4}{3} - \frac{4(2x-L)}{L} + \frac{4(2x-L)^2}{L^2} - \frac{4(2x-L)^3}{3L^3} & \frac{3L}{4} \le x \le L \end{cases} \tag{4}$$

If w is substituted into the nonlinear total potential energy function, V, of Eqs. (1) and (2) it becomes explicitly:

$$V(Q,L) = \frac{512EI}{3L^3}Q^2 - \frac{4P}{3L}Q^2 + \frac{151kL}{2520}Q^2 + \frac{4\chi\mu qt}{3}|Q| + \frac{40853}{4324320}CQ^4L \tag{5}$$

3.2.1. The linearised solution ($C=0$)

When $C=0$ the nonlinearity in the foundation is absent and we can directly follow the Galerkin analysis of Budd et al. (2003). The optimum buckle length is obtained by minimizing V with respect to L, giving

$$L_{\text{opt}} = \sqrt{\frac{48\sqrt{1225P^2 + 84560kEI} - 1680P}{151k}} \tag{6}$$

Note that L_{opt} does not depend upon the amplitude Q in this case. Equilibrium states (which necessarily correspond to functions with w, $\dot{w}$ and $\ddot{w}$ all zero at the ends) are found by seeking stationary values of V with respect to Q ($\partial V/\partial Q = 0$) to give:

$$Q = \pm\frac{1680\chi\mu qtL^3}{3360PL^2 - 430080EI - 151kL^4} \tag{7}$$

Combining these two results gives the equilibrium states of Fig. 6, which, qualitatively, are very close in form to those in

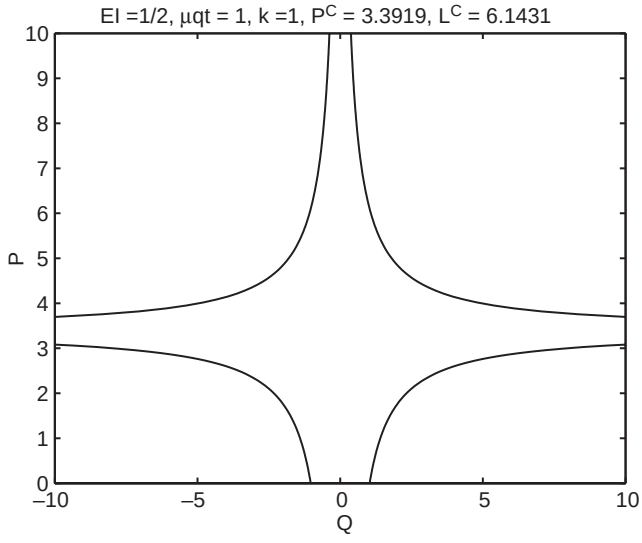

Fig. 6. Bifurcation diagram for one-spline model, linear foundation.

Budd et al. (2003), but relate inherently to a single hump rather than the periodic response.

The critical load P^C and related length L^C can be found by substituting L_{opt} into the second derivative of V with respect to Q and setting the result to zero ($\partial^2 V/\partial Q^2 = 0$) (Thompson and Hunt, 1973) to give

$$P^C = \sqrt{\frac{2416}{105}kEI}; \quad L^C = 8\sqrt[4]{\frac{105}{151}\frac{EI}{k}} \tag{8}$$

3.2.2. The nonlinear solution ($C \neq 0$)

The same sequence of arguments can be applied to the case of $C \neq 0$, although the presence of the nonlinearity makes solution more difficult. First minimizing V with respect to L gives

$$L_{opt} = \sqrt{\frac{192\sqrt{15015(15015P^2 + 1036464EIk + 163412EICQ^2)} - 2882880P}{259116k + 40853CQ^2}} \tag{9}$$

We note that L is now not only a function of the load P, but also of the amplitude Q. This is fundamentally different from the notion conceived by Biot that the wavelengths change during fold evolution, as Eq. (9) relates inherently to a single hump and not to a wavetrain as suggested by the 'dominant' wavelength analysis (Biot, 1961).

The equilibrium equation $\partial V/\partial Q = 0$ becomes

$$\frac{\partial V}{\partial Q} = \frac{1024EI}{3L^3}Q - \frac{8P}{3L}Q + \frac{151kL}{1260}Q \pm \frac{4}{3}\chi\mu qt + \frac{40853CL}{1081080}Q^3 = 0 \tag{10}$$

For $P > P^C$ and each L, there are three possible solutions of Eq. (10) for Q. The solutions of Eqs. (9) and (10) can be found by iteration of L and Q. The linear approximation for L_{opt} given by Eq. (6) is first substituted into Eq. (10) and then each of the three possible solutions for Q thus obtained is substituted in turn into Eq. (9) to update the approximations for L_{opt}. The process is continued until convergence is achieved.

Fig. 7 shows how a single fold evolves far into the post-buckling range, highlighting the variation of buckle length L and amplitude Q with load P as the solution destabilizes and restabilizes again. Also, the upper right quadrant of the bifurcation diagram for several values of C is seen in Fig. 8, detailing how the restabilization is affected by the degree of nonlinearity.

4. Two B-spline formulation

In experiments used to mimic parallel folding, humps are commonly observed to form sequentially, i.e. by serial folding. To explore this multiple hump scenario in the simplest manner, we next consider a two-spline formulation allowing for two independent maxima/minima. Using this two-spline formulation, we find that the model has more freedom to select the waveshape, rather than the Galerkin approximation, which imposes the profile. To this end, we take values of $C > 0$ for loads above P^C, such that restabilization of the foundation and the consequent lock-up in amplitude can successfully model the response of the experiments of Fig. 1.

The wave pattern is represented by two rescaled cubic B-splines w_1 and w_2 with amplitudes Q_1 and Q_2 and lengths L_1 and L_2, respectively. The full deflection w along the wave is then found by superposition of w_1 and w_2. Both primitive periodic ($Q_2 = -Q_1$) and localized ($Q_2 \neq -Q_1$) solutions are found to co-exist (see Fig. 9). Note that due to the interference of w_1 and w_2, in most cases the maximum and minimum amplitudes of w will differ from Q_1 and Q_2.

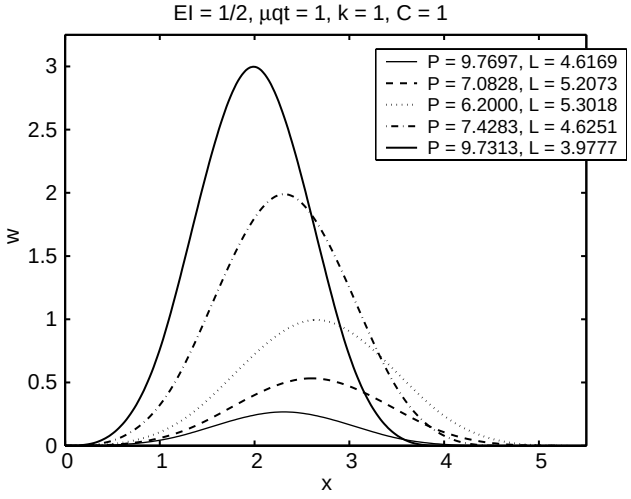

Fig. 7. Wave profiles for one-spline model, nonlinear foundation.

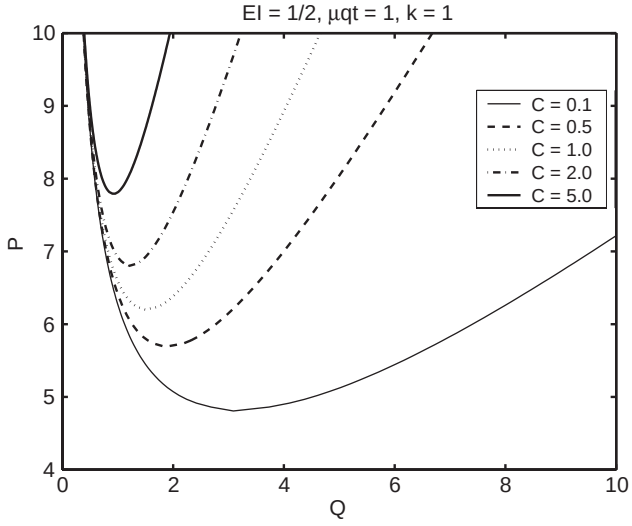

Fig. 8. Bifurcation diagram for the nonlinear one-spline model when $P > P^C$, for differing C values.

Fig. 9. Schematic representation of primitive modeshapes from the two B-spline model: (a) homoclinic ($Q_1 \neq -Q_2$); (b) periodic ($Q_1 = -Q_2$).

4.1. Overlap

If the wave is modelled in this way, then it is necessary to consider how much w_1 and w_2 should interfere. To this end we introduce an overlap variable, $0 \leq \Omega \leq 1$, such that ΩL represents the position along the first spline where the second spline starts: $\Omega = 0$ thus implies complete overlap and $\Omega = 1$ implies no interference at all. For the intervals $0 \leq \Omega \leq 1/4$, $1/4 \leq \Omega \leq 1/2$, $1/2 \leq \Omega \leq 3/4$ and $3/4 \leq \Omega \leq 1$ different sections of w_1 are superposed with w_2 and the total length $(\Omega L_1 + L_2)$ must be split up accordingly. Later we will minimize the maximum total potential energy with respect to Ω. It is worth commenting that Ω helps to dictate the overall length of the buckled region and hence removes some of the importance of the influence of L_1 and L_2.

4.2. Galerkin model

The two-spline model has a total of five degrees of freedom, amplitudes Q_i $(i = 1, 2)$, their corresponding lengths L_i, and overlap Ω. Ideally, energy minimization should be carried out with respect to each of these variables independently. However, the resulting process was considered unnecessarily cumbersome and for the present descriptive purposes it was found more instructive to reduce the description to the two underlying variables Q_1 and Q_2, such that the contour plots of the following section could be drawn. This was done first by taking the spline lengths directly from the nonlinear single spline result (9), and secondly minimizing only once at each load value with respect to Ω, under the periodic assumption $Q_1 = -Q_2$. Whilst noting that the localized solutions $Q_1 \neq -Q_2$ could possibly lead to slightly different overlap values if complete freedom were allowed, the two sets of results were not expected to differ to any great extent.

4.3. Results

Having reduced the potential energy to two degrees of freedom, the energy function at any particular load level can be visualized as a two-dimensional surface $V(Q_1,Q_2)$. The stationary values—maxima, minima and saddle points—of this surface then correspond to states of equilibrium. In the regime of *overall negative stiffness*, where the load is dropping as the end-shortening increases and hence the layers are softening, the solutions will be *unstable* (Timoshenko and Gere, 1961). Hence the least energy solution is the minimum of a local maximum or a saddle point. Although it is possible for a system to get stuck in a local minimum, in the following it shall be assumed that equilibrium states with the lowest energy will provide the preferred modeshapes.

Taking the parameter values $\chi\mu qt = 1$, $EI = 1/2$, $k = 1$ and $C = 1$, the equilibrium solutions can be found either by varying P or by varying the end-shortening Δ. In Fig. 10 we present the results of a series of such calculations, taking an initially large load P and successively reducing it in value. This shows an interesting transition in the preferred modeshape. For P greater than a value of $P \approx 6.5$ the preferred modeshape is a localized solution with effectively just one hump, whereas for P less than this value a second hump starts to develop. Localized solutions are found to be preferred at high load levels, much like the single spline solution, with a transition taking place to the periodic solutions as the load level falls. This therefore successfully models an early stage of the experimental sequence seen in Fig. 1.

We can understand the nature of this transition by studying the way that the contour surfaces of V change as P (or Δ) is altered. For $P > 6.5$ the contour surface has four saddle points and two maxima, corresponding to co-existing periodic and localized solutions, of which the localized solutions have the lowest energy. At $P \approx 6.5$ these maxima and saddle points start to coalesce, so that for $P < 6.1$ only two saddle points remain, corresponding now to the existence of low energy periodic solutions. Thus in a 'least energy' sense *serial buckling is a more likely phenomenon than a spontaneous wavetrain*. If having two synchronous humps was the preferred solution, then the periodic solutions found at the maxima would have the lowest energy. This process is examined further in Fig. 11, which compares the energy levels in the two possible equilibrium states. The comparative energy levels show that where the two curves differ, the localized solution is clearly preferred. However, the stiffness of the localized solution, although negative, has a slightly higher numerical value than that of the periodic. This contrasts with other structural situations, where a lower post-buckling stiffness often indicates the preferred solution (Hunt, 1989).

Looking more closely at the structure of contour plots, Fig. 12 shows the energy contours for a high load level, $P = 8$. This shows both saddle points and maxima, all of which are stationary solutions. It can be observed that at this constant load, all non-trivial equilibrium states have the same value of end-shortening, $\Delta = 0.098$, illustrated by the thick elliptical line. Apart from the apparent minimum of energy in the flat state $Q_1 = Q_2 = 0$, which lies within the jammed region of Fig. 4 and hence is of no practical significance, there are two equilibrium states of immediate interest. We have first the maximum of energy $V \approx 0.444$ lying in two positions on the $Q_1 = -Q_2$ line at $Q_1 \approx \pm 0.4$, representing the primitive periodic solution. Second, there is the saddle-point at $V \approx 0.3915$ occurring in four positions at $Q_1 \approx \pm 0.6$ with Q_2 very small, and again with $Q_2 \approx \pm 0.6$ and Q_1 very small. These

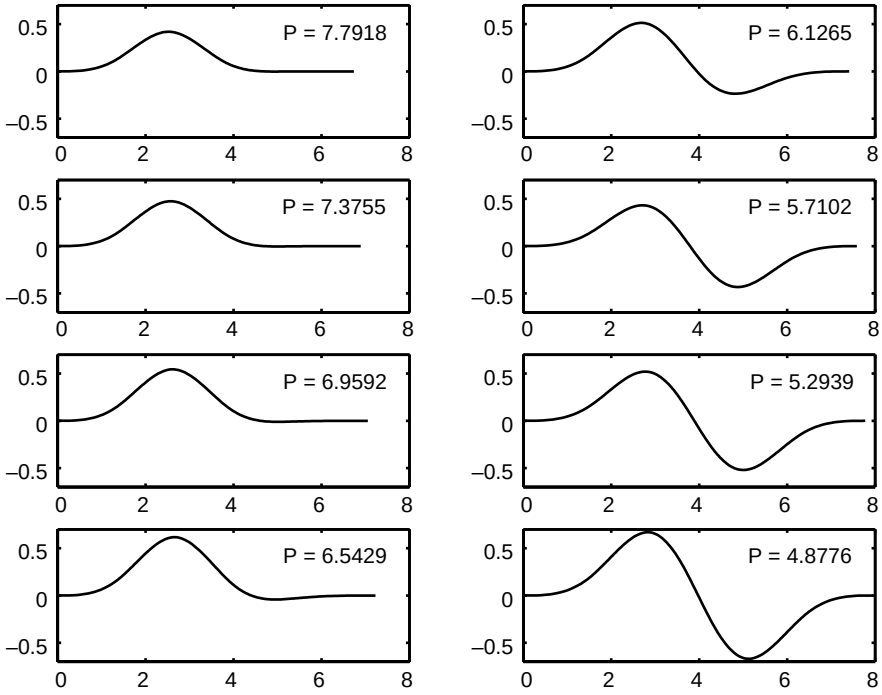

Fig. 10. Changes in preferred modeshape as the load drops and the end-shortening increases.

are the primitive homoclinic solutions. Interestingly, as both the maxima and the saddle points appear on the same end-shortening contour, at this value of Δ the release of strain energy suggested by the different energy levels takes place without any change in load.

Fig. 13 shows the energy contours for $P=6.1265$ and an end-shortening contour for $\Delta=0.25$. This has the same topological features as Fig. 12, except that two saddle points have converged on each maximum to the point where all three are about to become a single saddle on the $Q_1=-Q_2$ line. Note that the three states now take slightly different values of Δ at this load level, indicating that an instability would be accompanied by a drop in load. The conjunction of the three states of equilibrium is seen to take place at just about the same load level as the single-spline model for $C=1$ starts to restabilize (see Fig. 8). At this stage in the loading sequence, the system is starting to find it easier to take the periodic rather than the localized shape.

At around $P=4.6$, we find the minimum possible load, or nadir, of the equilibrium path. Here the single remaining saddle point converges with the minimum of V that represents the far-field restabilized periodic buckled state which appears outside of the illustrated range of Figs. 12 and 13 (see Fig. 15 in the next section for a clearer view of the transition between the load levels). The eventual restabilization for the periodic state thus takes place very much like that of Fig. 8 for the single spline, only at lower load levels.

The sequence described in the contour plots, taking place under falling load but increasing applied end-shortening, involves the preferred modeshape changing from localized to periodic as seen experimentally. This is further illustrated in the plots of Fig. 10, which shows this smoothly varying sequence over almost the complete range of loads from $P=8$, shown in the contour plot of Fig. 12, to the minimum load at $P\approx4.6$. The sequence could clearly be extended to further humps of buckling with the inclusion of extra splines.

4.4. Primitive periodic solution ($Q_2=-Q_1$)

The primitive two-spline periodic solution, given by $Q_2=-Q_1$, has been seen on the contour plots of Figs. 12 and 13. We next explore these particular solutions in more depth, starting with a description of the selection process for the value of Ω used in the plots. Fig. 14 show contours of Q_1 against Ω for this solution, at the highest load level used earlier.

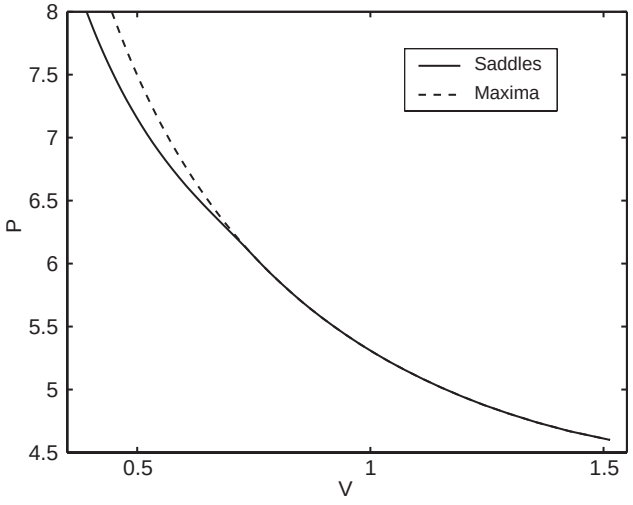

Fig. 11. Comparative variations of total energy V with P for both the $Q_2=-Q_1$ and the $Q_2\neq-Q_1$, noting the coalescence of these curves at $P\approx6.1$.

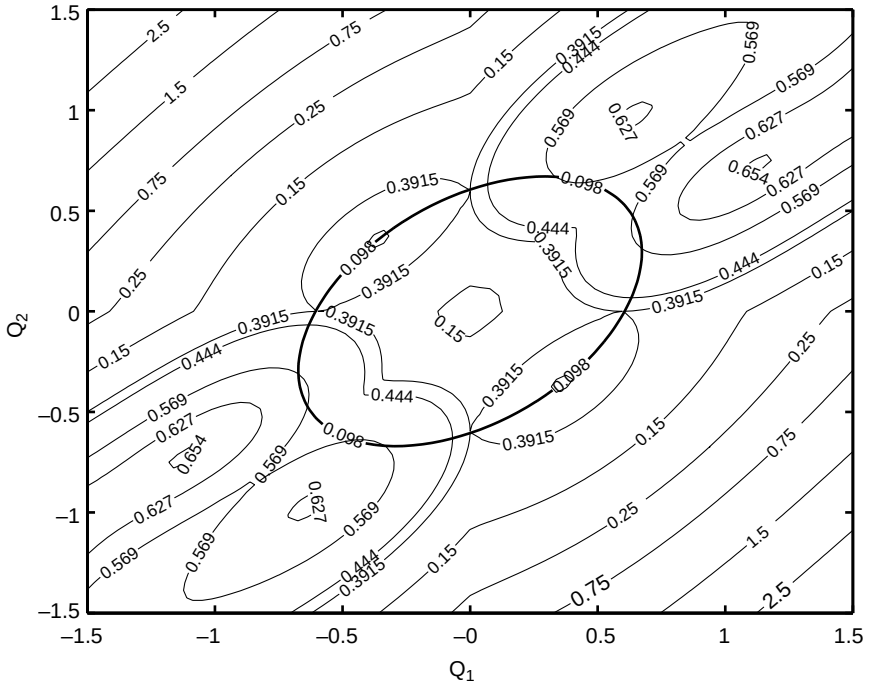

Fig. 12. Energy, V, and end-shortening, Δ, contour plot for Q_1-Q_2 space when $P=8$.

At higher loads, a single saddle point in V, specifically a minimum with respect to Ω and a maximum with respect to $Q_1(-Q_2)$, is clearly visible. At the minimum possible post-buckling load $P\approx 4.6$, this saddle point combines with the minimum energy state from the restabilized path and vanishes. Fig. 15 plots the energy variation with respect to Q_1 across the saddle point, at the three load levels. This illustrates again the transition from an energy shape with both a maximum and minimum, to one where there is no stationary point or equilibrium state.

The position of the saddle points can be determined numerically by transforming them into minima as follows. We start by reducing energy function $V(Q_1,\Omega)$ to just two degrees of freedom, by setting $Q_2=-Q_1$ and the load to be

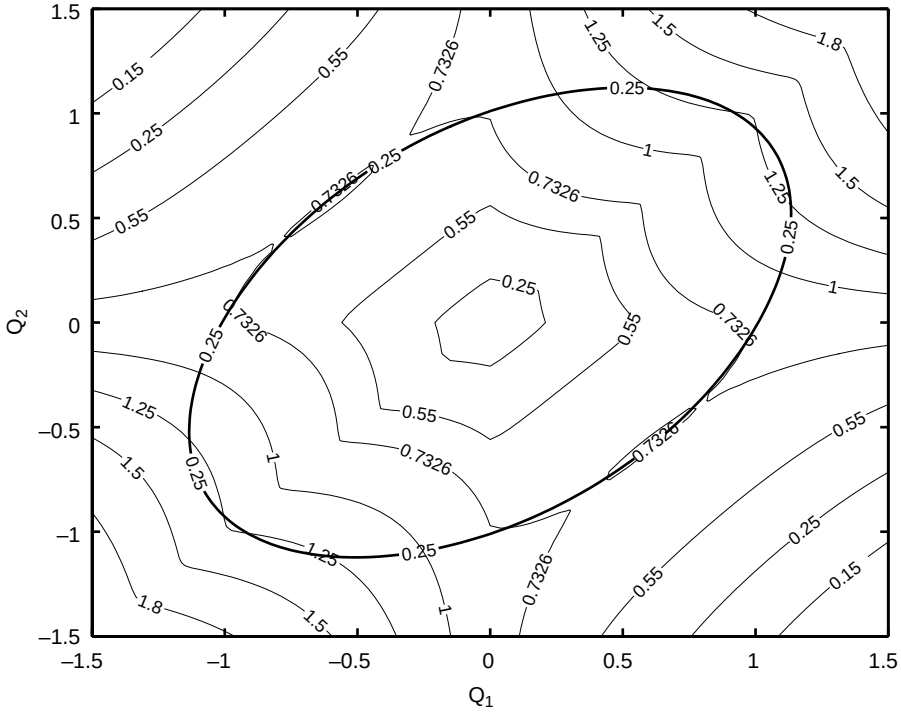

Fig. 13. Energy, V, and end-shortening, Δ, contour plot for Q_1-Q_2 space when $P=6.1265$.

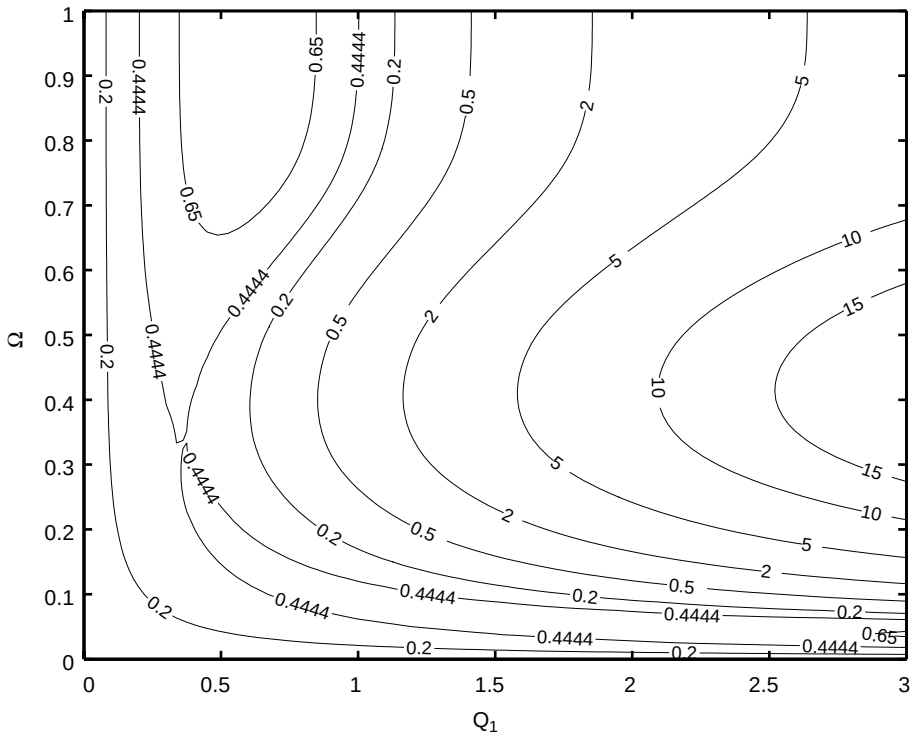

Fig. 14. Energy contour plot in $Q_1-\Omega$ space when $Q_2=-Q_1$ for $P=8$.

constant. If we then define the function:

$$F=\left(\frac{\partial V}{\partial Q_1}\right)^2+\left(\frac{\partial V}{\partial \Omega}\right)^2 \tag{11}$$

it becomes a relatively simple exercise to demonstrate that saddles in V convert to minima in F (Hunt et al., 2004), a schematic of which is shown in Fig. 16.

Using the MATLAB command *fminsearch*, which performs unconstrained nonlinear optimization (The Math Works, 2001), with an educated initial guess for the values of Q_1 and Ω at $P=8$ from Fig. 14, we can converge to the correct values at the saddle point. These can then be used for the initial guess at the next load level.

Fig. 17 shows variations of amplitude, overlap and end-shortening for the $Q_2=-Q_1$ solution, over the post-buckling regime where the load falls while the end-shortening increases. Note that qualitatively the first of these is again similar to the periodic analysis given by Budd et al. (2003).

4.5. Primitive localized solution ($Q_2\neq -Q_1$)

With Ω found at each load level, using Fig. 12, initial estimates for the values of Q_1 and Q_2 at the saddle points when $P=8$ can be made. To locate the saddle points of V, the same method used in the previous subsection to search $Q_1-\Omega$ space is adopted, with the role of Ω replaced by Q_2.

Fig. 18 shows variations of the spline amplitudes Q_1 and Q_2, and the maximum and minimum displacements along the length (combinations of Q_1 and Q_2) over the same post-buckling load range as Fig. 17. Both plots show a fall in the greater of the two values accompanied by an increase in the smaller value, as the preferred equilibrium state changes from localized to periodic, i.e. the initial fold decreases as the second fold grows. This process is examined further in Fig. 19, which compares the end-shortening values in the two possible equilibrium states. At $P\approx 6.4$, part of the falling saddle-point curve apparently turns back on itself, which corresponds to the drop in the value of Q_1. Such behaviour would not normally be obtainable experimentally, even under conditions of controlled end-shortening. The actual response would be marked by a sudden downwards drop in load, at the constant value of Δ (and hence Q_1) marked by the point of vertical tangency of the load/end-shortening curve. This same phenomenon is familiar from

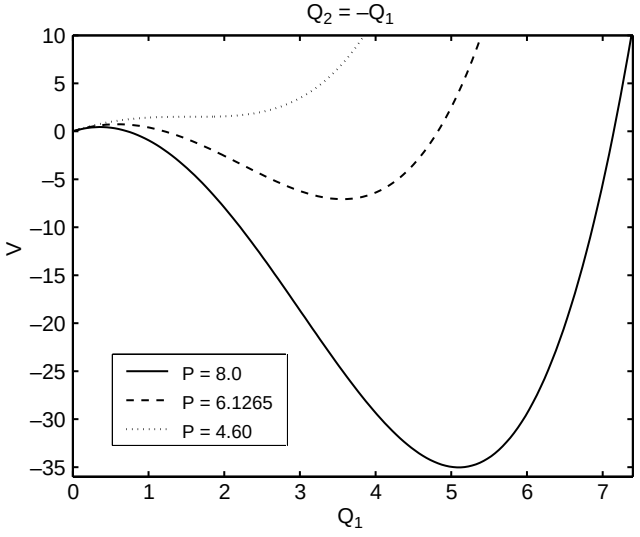

Fig. 15. Energy profile when $Q_2=-Q_1$ for $P=8$, $P=6.1265$ and $P=4.6$.

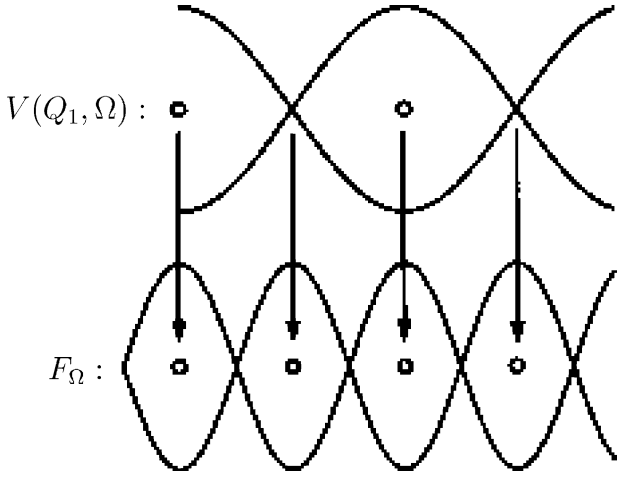

Fig. 16. Schematic representation of transformation from $V(Q_1,\Omega)$ to F_Ω.

a number of related structural problems and has been termed *snap-back* behaviour. It is often, even in paper samples, marked by an audible bang (Wadee et al., 2004) as significant strain energy is released.

5. Concluding remarks

The model of Budd et al. (2003) for the non-linear buckling of a confined two-layer system with episodical bedding plane slip, by virtue of its use of periodic boundary conditions, in the geological context is applicable only to synchronous folding. By introducing the less restrictive cubic B-splines into the potential energy formulation, we have developed a rigorous analysis of two-stage serial folding and we can thus mimic the behaviour that has been established as a common phenomenon in the parallel folding of rocks. As a direct consequence, we see that non-synchronous folding is the preferred solution when compared with spontaneous buckling.

In addition to providing the first theoretical treatment of serial folding, the theory presented in this paper also predicts that slip between the layers during folding will occur in a series of slip events rather than at a uniform rate. This stick-slip process has long been recognised in nature and characterises the movement along faults and along bedding planes during flexural slip folding, in the upper parts of the crust. These episodes of slip are sometimes recorded as multiple layers of crystal fibres (commonly calcite or quartz) that accumulate along the bedding planes.

In considering the rheology of rocks during folding as elastic and using energy considerations, it has been shown that the finite amplification of individual humps is inherent in the formulation. This justifies the validity of the model over earlier viscous models, which were based on the synchronous formation of folds in a wave-train.

The use of elastic buckling theories to account for geological folding does, however, require some justification. Geological folding results in the permanent deformation of the rock layers and it follows that the layers have behaved in a non-elastic manner. However, it is argued that this does not

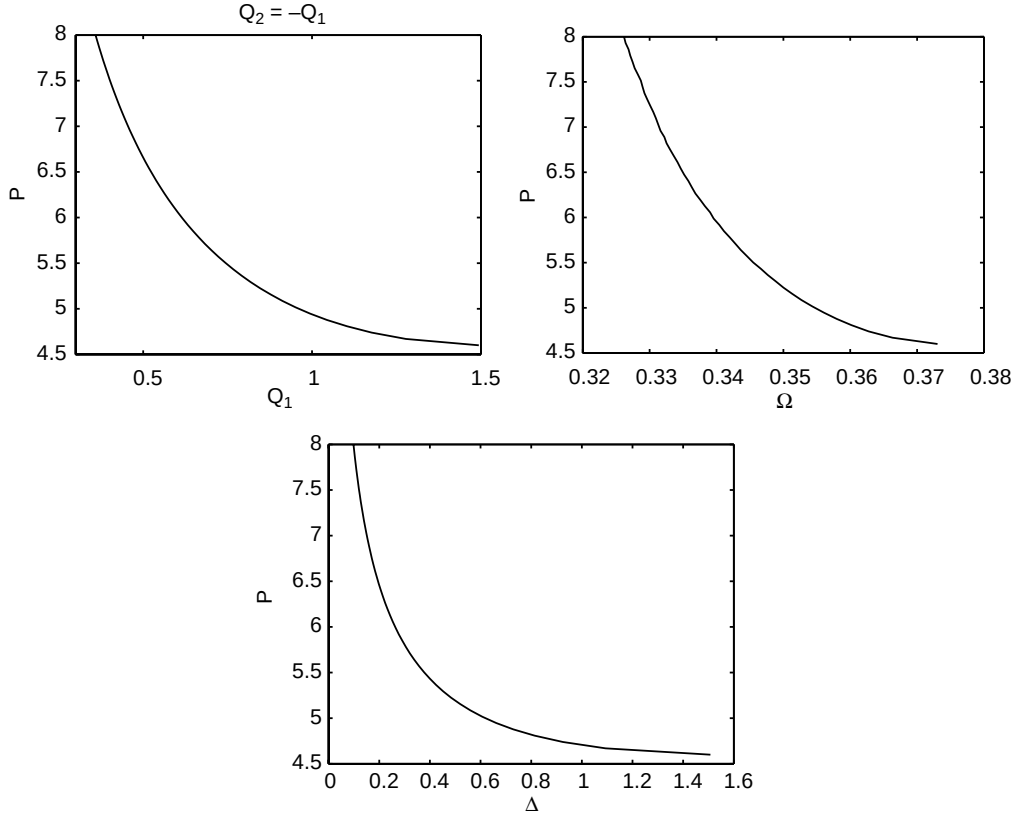

Fig. 17. Variations of amplitude, Q_1, overlap, Ω, and end-shortening, Δ, with load, P, for the $Q_2 = -Q_1$ solution.

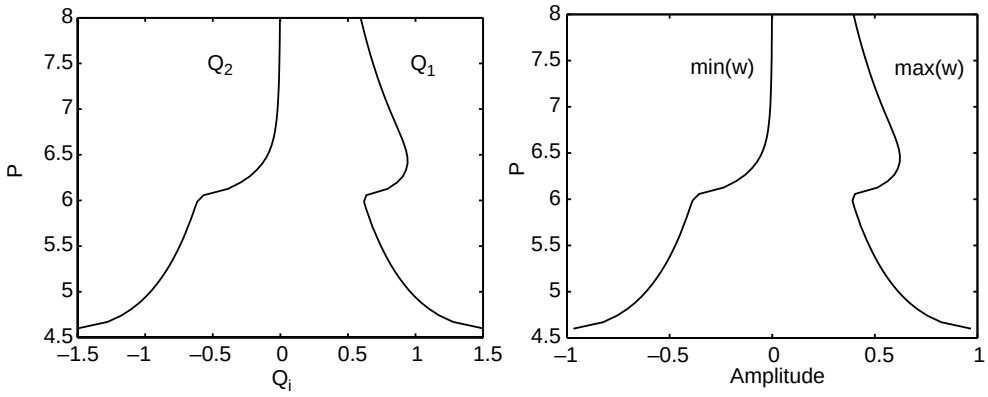

Fig. 18. Variations of amplitudes, Q_1 and Q_2, and maximum and minimum displacements, w_{max} and w_{min}, with P for the $Q_2 \neq -Q_1$ solution.

invalidate the use of elastic theories to describe geological folding. We suggest that folding, particularly in the upper crust, could be initiated by elastic buckling and only subsequently, as the fold amplifies beyond the elastic limit, may other rheological properties dominate the deformation.

The fact that the load continues to fall as the buckling changes from a single localized hump to the two-hump 'periodic' fold apparently contrasts with earlier work detailing similar behaviour. Usually it would be expected that the propagation of the stress to form additional humps in a progression would be marked by the load periodically falling and rising (Hunt et al., 2000; Budd et al., 2001; Wadee et al., 2004). It yet remains to be seen, however, whether this loading pattern would persist if more than two contributing cells were included.

The present formulation is, of course, limited and there are two clear ways in which it might be developed further. First, a recent contribution has extended it to a multilayer model comprising N layers and compared the results with experiments (Edmunds et al., in press). Second, having two sequential folds is clearly inadequate for the modelling of an entire serial folding sequence. Whilst adding extra cubic B-splines to the problem will rapidly increase the computational complexity, it could be of interest to adapt the splines formulation to uncover the process of development of the nth fold, after assuming that $n-1$ have already formed. This should be possible with just a slight modification of boundary conditions at one end of one of the splines.

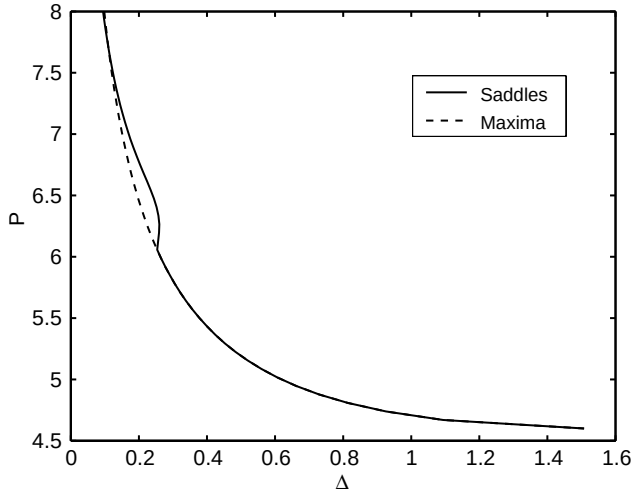

Fig. 19. Comparative variations of end-shortening, Δ, with P for both the $Q_2 = -Q_1$ and the $Q_2 \neq -Q_1$, noting the coalescence of these curves at $P \approx 6.1$.

Acknowledgements

The authors would like to thank Dr John-Paul Latham from the Department of Earth Science and Engineering at Imperial College, London for his valuable advice and comments as regards the geological content in this paper.

References

Biot, M.A., 1961. Theory of folding of stratified viscoelastic media and its implication in tectonics and orogenesis. Bulletin of the Geological Society America 72, 1595–1620.

Biot, M.A., 1963. Theory of stability of multilayered continua in finite, anisotropic elasticity. Journal of the Franklin Institute 276 (2), 128–153.

Biot, M.A., 1964. Theory of internal buckling of a confined multilayered structure. Bulletin of the Geological Society America 75, 563–568.

Blay, P., Cosgrove, J.W., Summers, J.M., 1977. An experimental investigation of the development of structures in multilayers under the influence of gravity. Journal of the Geological Society London 133, 329–342.

Budd, C.J., Hunt, G.W., Kuske, R., 2001. Asymptotics of cellular buckling close to the Maxwell load. Proceedings of the Royal Society London A 457, 2935–2964.

Budd, C.J., Edmunds, R., Hunt, G.W., 2003. A nonlinear model for parallel folding with friction. Proceedings of the Royal Society London A 459, 2097–2119.

Champneys, A.R., Hunt, G.W., Thompson, J.M.T. (Eds.), 1999. Localization and Solitary Waves in Solid Mechanics. World Scientific Publishing, Singapore.

Cobbold, P.R., 1975. Fold propagation in single embedded layers. Tectonophysics 27, 333–351.

de Sitter, L.U., 1964. Structural Geology. McGraw-Hill, New York.

Edmunds, R., Hunt, G.W., Wadee, M.A., 2006. Parallel folding in multilayered structures. Journal of Mechanics and Physical Solids 54 (2), 384–400.

Hobbs, B.E., Means, W.D., Williams, P.F., 1976. An Outline of Structural Geology. Wiley, New York.

Hunt, G.W., 1989. Bifurcation of structural components. Proceedings of the Institution of Civil Engineers Part 2 87, 443–467.

Hunt, G.W., 2006. Buckling in space and time. Nonlinear Dynamics, in press.

Hunt, G.W., Peletier, M.A., Champneys, A.R., Woods, P.D., Wadee, M.A., Budd, C.J., Lord, G.J., 2000. Cellular buckling in long structures. Nonlinear Dynamics 21 (1), 3–29.

Hunt, G.W., Hu, B., Butler, R., Almond, D.P., Wright, J.E., 2004. Nonlinear modeling of delaminated struts. AIAA Journal 42 (11), 2364–2372.

Johnson, A.M., 1977. Styles of Folding. Elsevier, Amsterdam.

Latham, J.-P., 1985a. The influence of nonlinear material properties and resistance to bending on the development of internal structures. Journal of Structural Geology 7 (2), 225–236.

Latham, J.-P., 1985b. A numerical investigation and geological discussion of the relationship between folding, kinking and folding. Journal of Structural Geology 7 (2), 237–249.

Price, N.J., 1970. Laws of rock behaviour in the Earth's crust. In: Sommerton, W.H. (Ed.), Rock Mechanics—Theory and Practice Proceeding of 11th Symposium of Rock Mechanics. A.I.M.M., pp. 3–23. Chapter 1.

Price, N.J., 1975. Rates of deformation. Journal of the Geological Society London 131, 553–575.

Price, N.J., Cosgrove, J.W., 1990. Analysis of Geological Structures. Cambridge University Press.

Ramberg, H., 1961. Contact strain and folding instability of amultilayered body under compression. Geologisches Rundschau 51, 405–439.

Ramberg, H., 1964. Selective buckling of composite layers with contrasted rheological properties; a theory for simultaneous formation of several orders of folds. Tectonophysics 1, 307–341.

The Math Works, Inc., 2001. MATLAB: high-performance numeric computation and visualization software. Natick, MA, USA: The Math Works Inc. Version 6.1, Release 12.1.

Thompson, J.M.T., Hunt, G.W., 1973. A General Theory of Elastic Stability. Wiley, London.

Timoshenko, S.P., Gere, J.M., 1961. Theory of Elastic Stability. McGraw-Hill, New York.

Wadee, M.A., Hunt, G.W., Peletier, M.A., 2004. Kink band instability in layered structures. Journal of Mechanical and Physical Solids 52 (5), 1071–1091.